Geophysical Journal International

Geophys. J. Int. (2010) doi: 10.1111/j.1365-246X.2010.04773.x

Tube wave signatures in cylindrically layered poroelastic media computed with spectral method

Florian Karpfinger,[1]* Boris Gurevich,[2,3] Henri-Pierre Valero,[1]† Andrey Bakulin[4]‡ and Bikash Sinha[1]

[1] *Schlumberger-Doll Research, Boston, USA. E-mail: fkarpfinger@slb.com*
[2] *Curtin University of Technology Department of Exploration Geophysics, GPO Box* U1987, *Perth,* WA 6845, *Australia*
[3] *CSIRO Petroleum, Bentley, Western Australia*
[4] *WesternGeco, Houston, USA*

Accepted 2010 August 12. Received 2010 August 12; in original form 2009 March 9

SUMMARY

This paper describes a new algorithm based on the spectral method for the computation of Stoneley wave dispersion and attenuation propagating in cylindrical structures composed of fluid, elastic and poroelastic layers. The spectral method is a numerical method which requires discretization of the structure along the radial axis using Chebyshev points. To approximate the differential operators of the underlying differential equations, we use spectral differentiation matrices. After discretizing equations of motion along the radial direction, we can solve the problem as a generalized algebraic eigenvalue problem. For a given frequency, calculated eigenvalues correspond to the wavenumbers of different modes. The advantage of this approach is that it can very efficiently analyse structures with complicated radial layering composed of different fluid, solid and poroelastic layers. This work summarizes the fundamental equations, followed by an outline of how they are implemented in the numerical spectral schema. The interface boundary conditions are then explained for fluid/porous, elastic/porous and porous interfaces. Finally, we discuss three examples from borehole acoustics. The first model is a fluid-filled borehole surrounded by a poroelastic formation. The second considers an additional elastic layer sandwiched between the borehole and the formation, and finally a model with radially increasing permeability is considered.

Key words: Numerical solutions; Downhole methods; Guided waves; Wave propagation; Acoustic properties.

1 INTRODUCTION

Modelling propagation of various wave modes in a fluid-filled borehole is an important step in evaluating formation properties. Various modes propagate in a fluid-filled borehole and are sensitive to different properties of the formation (White 1983; Paillet & Cheng 1991; Sinha & Zeroug 1997). One important aspect of modelling wave propagation in fluid-filled boreholes is the effect of poroelastic media on mode signatures. This interest is strongly linked to the oil industry and the need to estimate the fluid mobility in reservoirs. Beyond the scope of geophysical applications, the understanding of wave propagation in cylindrical poroelastic structures is of great importance in the areas of non-destructive testing, mechanical engineering and civil engineering.

Over the last three decades great efforts have been made to investigate wave propagation in poroelastic cylindrical structures. The effects of dispersion and attenuation in cylindrically layered poroelastic structures were investigated theoretically as well as experimentally. We give a short literature review on the work done for geophysical applications.

The first fundamental work on this subject was done by Biot and now is known as Biot's equations of poroelasticity (Biot 1956a,b, 1962). Then, framework for wave propagation in a fluid saturated poroelastic cylinder was provided by Gardner (1962) while the dispersion for the full range of frequencies for open and closed boundary conditions was studied by Berryman (1983). Later, White (1986) and Mörig & Burkhardt (1989) measured the dispersion of the extensional mode in laboratory experiments while Dunn (1986) wrote a review on extensional, torsional and flexural modes. Later, Berryman & Pride (2005) utilized torsional waves to estimate the effect of patchy saturation in a cylinder.

In addition to these general theoretical and experimental works, the need to estimate fluid mobility in reservoirs triggered studies on the so-called tube wave or Stoneley wave which propagates in

*Formerly at: Curtin University of Technology, Department of Exploration Geophysics, GPO Box U1987, Perth,WA 6845, Australia.
†Now at: Schlumberger SKK, Japan.
‡Now at: Saudi Aramco, Dharan, Saudi Arabia.

the fluid column of the borehole. A special characteristic of tube waves is their high sensitivity to the fluid mobility. The dispersion of tube waves propagating in boreholes surrounded by a poroelastic formation was used to invert for the mobility (Rosenbaum 1974; Chang *et al.* 1988; Schmitt *et al.* 1988; Norris 1989) while Sinha *et al.* (2006) proposed an approach to estimate the radial distribution of mobility. In addition to these theoretical developments, some laboratory-scale experiments have been conducted. This was modelled by using a hollow poroelastic cylinder submerged into a fluid (Liu 1988).

All the research work discussed above uses the traditional, analytic method often referred to as 'root-finding'. This method finds general solutions to the underlying equations, which are a combination of Bessel functions of different order. Substituting the solution into the boundary conditions yields a homogeneous system of linear algebraic equations. For this system to have non-trivial solutions, the determinant of its matrix must be equal to zero. This is called the frequency equation. The roots of this equation, which have to be found in the complex plane, yield the dispersion relation.

In this paper we introduce a new alternative approach based on the spectral method first used by Adamou & Craster (2004). The advantages of this approach are that it is easy to implement and the computational time is very fast. Karpfinger *et al.* (2008a, 2010) expanded the spectral method to axisymmetric waves for an arbitrary number of fluid and solid layers, while in this paper the same methodology is further applied to the poroelastic case. First, poroelastic equations in cylindrical coordinates are introduced together with their formulation in the spectral domain. Then boundary conditions for all possible poroelastic interfaces are discussed. Finally, three numerical examples are discussed. First, a borehole surrounded by a poroelastic formation with open and closed boundary conditions is used as a benchmark. The dispersion and attenuation are plotted for a range of permeabilities. Even though the formation parameter which can be estimated from the tube wave dispersion is the mobility, being the ratio of permeability to fluid viscosity, we will refer in this work to permeability as the viscosity of the pore fluid is chosen to be 10^{-3} Pa s for all calculations. In the second model, an additional elastic layer is introduced between the fluid and the poroelastic formation. This allows us to study the impact of the thickness of this layer on the dispersion of the tube wave. The third model illustrates the effect of an altered zone with a radial increase of the permeability.

2 THEORY

In this paper we study wave propagation in a fluid-filled borehole surrounded by a medium composed of fluid, elastic and poroelastic layers. Wave propagation in cylindrical, poroelastic structures is considered within the framework of Biot's theory of poroelasticity. In the next section Biot's theory for an infinite, poroelastic medium is reviewed. Fig. 1 illustrates a fluid-filled borehole surrounded by a poroelastic medium. The structure is infinite in the axial direction while in the radial one any combination of fluid, elastic and poroelastic layers can be considered. A radially infinite medium is modelled by choosing the outer layer to be much bigger than the borehole radius (we are considering a factor of 10 to be sufficient). Due to the geometry of the problem we are going to solve, the wave and the constitutive equations will be expressed using a cylindrical coordinate system. Throughout this paper the cylindrical coordinate system will be defined as follows: the z-axis will be aligned with the axis of the cylinder while r is the radial coordinate (see Fig. 1).

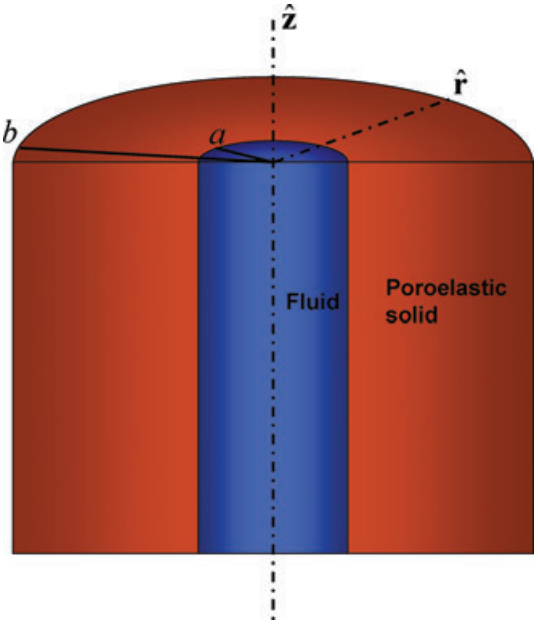

Figure 1. Example for a two-layer cylindrical structure: hollow poroelastic cylinder filled with fluid.

The motion is independent of the angular displacement. Thus, the particle motion happens in the $r - z$ plane only, involving radial and axial displacement. The angular displacement is assumed to be zero.

To simulate propagating modes in such a system we assume that a plane wave front is propagating parallel to the axis of the cylinder. Under these assumptions, stress and displacement components can be estimated for a multilayered system composed of a combination of poroelastic, fluid and elastic layers.

2.1 Biot's theory of poroelasticity: review

Waves propagating in an infinite poroelastic medium satisfy the following equations (Biot 1962):

$$\nabla \cdot \boldsymbol{\sigma} = -\omega^2(\rho \boldsymbol{u} + \rho_f \boldsymbol{w}), \tag{1}$$

$$\nabla p = \omega^2(\rho_f \boldsymbol{u} + q \boldsymbol{w}), \tag{2}$$

where the field variables are given as the bulk displacement $\boldsymbol{u}$ and the relative solid-fluid displacement $\boldsymbol{w} = \phi(\boldsymbol{U} - \boldsymbol{u})$ with ϕ being the porosity. $\boldsymbol{u}$ is the fluid displacement while ρ and ρ_f are the densities of porous material and the fluid, respectively. The frequency-dependent density term $q(\omega)$ is defined by Pride & Haartsen (1996) as

$$q(\omega) = \frac{\mathrm{i}}{\omega} \frac{\eta}{k(\omega)}, \tag{3}$$

where η is the viscosity and $k(\omega)$ the frequency-dependent permeability (Johnson *et al.* 1987). This complex density is responsible for the viscous and inertial coupling between the solid and fluid phases (Biot 1956b). The total stress tensor $\boldsymbol{\sigma}$ and the fluid pressure p are related to the field vectors by the constitutive equations

$$\boldsymbol{\sigma} = [(H - 2\mu)\nabla \cdot \boldsymbol{u} + \alpha M \nabla \cdot \boldsymbol{w}]\boldsymbol{I} + \mu[\nabla \boldsymbol{u} + \nabla \boldsymbol{u}^T], \tag{4}$$

$$p = -M \nabla \cdot \boldsymbol{w} - \alpha M \nabla \cdot \boldsymbol{u}. \tag{5}$$

In eqs (4) and (5) μ is the shear modulus of the solid frame while $\alpha = 1 - K/K_g$ is the Biot–Willis coefficient (Biot & Willis 1957).

K is the drained bulk modulus and K_g is bulk modulus of the grain material. The so-called pore space modulus is defined as

$$M = \left[\frac{\alpha - \phi}{K_g} + \frac{\phi}{K_f} \right]^{-1}, \tag{6}$$

where K_f is the fluid bulk modulus.

The P-wave modulus H of the saturated poroelastic medium is defined as follows

$$H = K_{\text{sat}} + \frac{4}{3}\mu\,, \tag{7}$$

where K_{sat} is the bulk modulus of the saturated medium which is related to the drained modulus K by the (Gassmann 1951) equation

$$K_{\text{sat}} = K + \alpha^2 M. \tag{8}$$

Substituting the constitutive relations eqs (4) and (5) into eqs (1) and (2), we obtain two coupled wave equations. To decouple these equations into Helmholtz equations for the three bulk waves propagating in an isotropic poroelastic medium, the displacements are written in terms of scalar and vector potentials as

$$\boldsymbol{u} = \nabla\Upsilon + \nabla \times \boldsymbol{\beta}, \quad \boldsymbol{w} = \nabla\psi + \nabla \times \boldsymbol{\chi}, \tag{9}$$

where Υ,ψ and $\boldsymbol{\beta}$, $\boldsymbol{\chi}$ are scalar and vector potentials, respectively,. Substituting eqs (9) into the two coupled wave equations yields for the shear wave

$$\left(\nabla^2 + \omega^2 s_s^2\right)\boldsymbol{\beta} = 0, \quad \chi = -\frac{\rho_f}{q}\boldsymbol{\beta}, \tag{10}$$

providing the expression for the shear wave slowness defined as

$$s_s^2 = \frac{\rho - \frac{\rho_f^2}{q}}{\mu}. \tag{11}$$

The wave equations for the two P waves in an infinite poroelastic medium are

$$\left(\nabla^2 + \omega^2 s_\pm^2\right) A_\pm = 0, \tag{12}$$

where the fast and slow P-wave slownesses are defined as

$$2s_\pm^2 = \frac{\rho M + qH - 2\rho_f C}{MH - C^2} \pm \sqrt{\left(\frac{\rho M + qH - 2\rho_f C}{(MH - C^2)}\right)^2 - \frac{4\left(q\rho - \rho_f^2\right)}{MH - C^2}}, \tag{13}$$

with the potential $A_\pm$ defined as

$$A_\pm = \Gamma_\pm \Upsilon + \psi, \tag{14}$$

where

$$\Gamma_\pm = \frac{\rho_f H - \rho C}{(MH - C^2)s_\pm^2 - (\rho M - \rho_f C)}. \tag{15}$$

C is a modulus defined as $C = \alpha M$. The equations derived above are valid for most kinds of coordinate systems.

2.2 Poroelastic equations in cylindrical coordinates

To apply Biot's theory for poroelastic media of cylindrical geometry, as might be expected it is more convenient to use cylindrical coordinates. For axisymmetric wave propagation, the subject of this work, the particle motion takes place solely in the $r - z$ plane. Thus the angular displacement u_θ equals zero. Under these assumptions, components of the stress–strain relations eq. (4) can be expressed as

$$\sigma_{rr} = (H - 2\mu)\Delta + 2\mu\frac{\partial u_r}{\partial_r} - \alpha M\zeta, \tag{16}$$

$$\sigma_{rz} = \mu\left(\frac{\partial u_r}{\partial_z} + \frac{\partial u_z}{\partial_r}\right), \tag{17}$$

where Δ is the dilation defined in cylindrical coordinates as

$$\Delta = \frac{\partial u_r}{\partial_r} + \frac{u_r}{r} + \frac{\partial u_z}{\partial_z}. \tag{18}$$

The fluid increment content is defined as $\zeta = -\nabla \cdot \boldsymbol{w}$. To distinguish between the torsional and extensional components of the wavefield, the potential $\boldsymbol{\beta}$ is further decomposed as

$$\boldsymbol{\beta} = \hat{\boldsymbol{z}}\beta_1 + \nabla \times (\hat{\boldsymbol{z}}\beta_2), \tag{19}$$

where $\hat{\boldsymbol{z}}$ is the unit vector in z-direction. Note that for axisymmetric modes only $\beta_2 \neq 0$. Eqs (9)–(19) describe axisymmetric wave propagation in a poroelastic cylinder.

2.2.1 Helmholtz equations

We are considering an infinite train of sinusoidal waves propagating along the z-axis of the cylinder. They are a harmonic function of z and t which take the form

$$A(r)_\pm = a_\pm(r)\mathrm{e}^{\mathrm{i}(k_z z - \omega t)}, \quad \beta(r)_2 = a_s(r)\mathrm{e}^{\mathrm{i}(k_z z - \omega t)}, \tag{20}$$

where ω is the angular frequency, k_z the axial wavenumber, and $a_\pm(r)$ and $a_s(r)$ are amplitude functions of r.

Using eqs (20) the wave equations (eqs 10 and 12) can be expressed in the $\omega - k_z$ domain as

$$\underbrace{\left(\partial_r^2 + r^{-1}\partial_r + \frac{\omega^2}{v_\pm^2}\right)}_{\mathfrak{L}_\pm} a_\pm = k_z^2 a_\pm, \tag{21}$$

$$\underbrace{\left(\frac{\partial^2}{\partial r^2} + \frac{1}{r}\frac{\partial}{\partial r} - \frac{1}{r^2} + \frac{\omega^2}{v_s^2}\right)}_{\mathfrak{L}_s} a_s = k_z^2 a_s. \tag{22}$$

The term $\mathrm{e}^{\mathrm{i}(k_z z - \omega t)}$ is omitted for clarity. The poroelastic Helmholtz equations are formulated similarly to the elastic case (Karpfinger *et al.* 2008a, section 1.B). Now the ordinary differential equations (eqs 21 and 22) contain derivatives only with respect to r and coefficients depending on frequency ω and axial wavenumber k_z. To find a relation between ω and k_z eqs (21) and (22) can be solved as an eigenvalue problem so that the wavenumber k_z^2 represents eigenvalues and the potentials $a_\pm$ and a_s are the eigenvectors. For linear elasticity it is possible to find a k_z for a given ω or vice versa (Adamou & Craster 2004). However, for poroelasticity it is advantageous to look for k_z as a function of ω as the bulk slowness (eqs 11 and 12) depends explicitly on ω.

The three Helmholtz equations of a poroelastic layer can be combined in a matrix equation that has the following form:

$$\underbrace{\begin{pmatrix} \mathfrak{L}_+ & 0 & 0 \\ 0 & \mathfrak{L}_{v_s} & 0 \\ 0 & 0 & \mathfrak{L}_- \end{pmatrix}}_{\mathfrak{L}_p} \underbrace{\begin{pmatrix} a_+ \\ a_s \\ a_- \end{pmatrix}}_{\boldsymbol{a_p}} = k_z^2 \begin{pmatrix} a_+ \\ a_s \\ a_- \end{pmatrix}. \tag{23}$$

To obtain the dispersion of propagating modes in multilayered cylindrical structures composed of poroelastic, elastic and fluid layers, eqs (21) and (22) plus the equivalent equations for fluid and solid layers need to be solved. A solution for such a system can only be found if the appropriate interface conditions for such a system are set. To apply the boundary or interface conditions, the displacements

and stress components have to be expressed independently of the axial wavenumber k_z to be able to formulate the problem where the eigenvalue is k_z. How this is achieved will be shown in the next section.

2.2.2 Displacement components

Displacement components need to be expressed independently of k_z. To achieve this, eq. (19) with $\beta_1 = 0$ and the expressions

$$\Upsilon = \frac{A_+ - A_-}{\Gamma_+ - \Gamma_-}, \qquad \psi = \frac{A_-\Gamma_+ - A_+\Gamma_-}{\Gamma_+ - \Gamma_-}, \tag{24}$$

are used to express the solid displacement $\boldsymbol{u}$ (eq. 9) as

$$\boldsymbol{u} = \underbrace{\frac{1}{\Gamma_+ - \Gamma_-}}_{\Gamma}\nabla A_+ - \underbrace{\frac{1}{\Gamma_+ - \Gamma_-}}_{\Gamma}\nabla A_- + \nabla \times (\nabla \times (\hat{z}\beta_2)). \tag{25}$$

The relative displacement can be written in a similar form to eq. (25) as

$$\boldsymbol{w} = -\Gamma_-\Gamma\nabla A_+ + \Gamma_+\Gamma\nabla A_- - \frac{\rho_f}{q}\nabla \times (\nabla \times (\hat{z}\beta_2)). \tag{26}$$

For three differential equations with three unknowns it is sufficient to use three displacement components: the radial u_r and axial u_z solid displacement components plus the radial w_r component of the relative displacement

$$u_r = \Gamma\partial_r a_+ - a_s - \Gamma\partial_r a_-, \tag{27}$$

$$\bar{u}_z = -\Gamma\underbrace{k_z^2 a_+}_{\mathfrak{L}_+ a_+} + \left(\partial_r + \frac{1}{r}\right)a_s + \Gamma\underbrace{k_z^2 a_-}_{\mathfrak{L}_- a_-}, \tag{28}$$

$$w_r = -\Gamma_-\Gamma\partial_r a_+ + \frac{\rho_f}{q}a_s + \Gamma_+\Gamma\partial_r a_-, \tag{29}$$

where $a_s = \mathrm{i}k_z a_s$ and $\bar{u}_z = \mathrm{i}k_z u_z$. These equations reduce to elasticity for $a_- = 0$, $\Gamma = 1$ and $w_r = 0$ (see eqs 13 and 14 and Karpfinger *et al.* 2008a).

The displacement components of a poroelastic layer are combined in the following matrix equation:

$$\begin{pmatrix} u_r \\ u_z \\ w_r \end{pmatrix} = \underbrace{\begin{pmatrix} \mathfrak{T}^+_{u_r} & \mathfrak{T}^s_{u_r} & \mathfrak{T}^-_{u_r} \\ \mathfrak{T}^+_{u_z} & \mathfrak{T}^s_{u_z} & \mathfrak{T}^-_{u_z} \\ \mathfrak{T}^+_{u_r} & \mathfrak{T}^s_{u_r} & \mathfrak{T}^-_{w_r} \end{pmatrix}}_{\mathfrak{T}_p} \cdot \begin{pmatrix} a_+ \\ a_s \\ a_- \end{pmatrix}, \tag{30}$$

where the matrix $\mathfrak{T}_\mathfrak{p}$ is composed of the coefficients of the displacement potential obtained from eqs (27)–(29). These coefficients will be discretized using differentiation matrices as will be explained later on.

2.2.3 Stress components

Stress components σ_{rr}, σ_{rz} and the fluid pressure p can now be written as functions of the potentials $a_\pm$ and a_s. For the radial stress we get the following expression:

$$\begin{aligned}\sigma_{rr} = {} & 2\mu\Gamma\partial_r^2 a_+ - (H - 2\mu)\Gamma\frac{\omega^2}{v_+^2}a_+ + C\Gamma\Gamma_-\frac{\omega^2}{v_+^2}a_+ - 2G\partial_r a_s \\ & - 2\mu\Gamma\partial_r^2 a_- + (H - 2\mu)\Gamma\frac{\omega^2}{v_-^2}a_- - C\Gamma\Gamma_+\frac{\omega^2}{v_-^2}a_- .\end{aligned} \tag{31}$$

The shear stress is expressed as

$$\begin{aligned}\bar{\sigma}_{rz} = {} & -2\mu\Gamma\left(\partial_r^3 + \frac{1}{r}\partial_r^2 - \frac{1}{r^2}\partial_r + \partial_r\frac{\omega^2}{v_+^2}\right)a_+ \\ & + \left[2\mu\left(\partial_r^2 + \frac{1}{r}\partial_r - \frac{1}{r^2}\right) + \rho\omega^2\right]a_s \\ & + 2\mu\Gamma\left(\partial_r^3 + \frac{1}{r}\partial_r^2 - \frac{1}{r^2}\partial_r + \partial_r\frac{\omega^2}{v_-^2}\right)a_- ,\end{aligned} \tag{32}$$

while for the fluid pressure (compare eq. 5) we get

$$\begin{aligned}-p = {} & \left[-M\Gamma\Gamma_-\frac{\omega^2}{v_+^2} + C\Gamma\frac{\omega^2}{v_+^2}\right]a_+ \\ & + \left[M\Gamma\Gamma_+\frac{\omega^2}{v_-^2} - C\Gamma\frac{\omega^2}{v_-^2}\right]a_- ,\end{aligned} \tag{33}$$

where $\bar{\sigma}_{rz} = \mathrm{i}k_z\sigma_{rz}$. Note that eqs (31)–(33) are derived from eqs (16), (17) and (5) by substituting the displacement components eqs (27)–(29).

Stress components are expressed in a matrix form similarly to the displacement components

$$\begin{pmatrix} \sigma_{rr} \\ \sigma_{rz} \\ -p \end{pmatrix} = \underbrace{\begin{pmatrix} \mathfrak{S}^+_{\sigma_{rr}} & \mathfrak{S}^s_{\sigma_{rr}} & \mathfrak{S}^-_{\sigma_{rr}} \\ \mathfrak{S}^+_{\sigma_{rz}} & \mathfrak{S}^s_{\sigma_{rz}} & \mathfrak{S}^-_{\sigma_{rz}} \\ \mathfrak{S}^+_{-p} & \mathfrak{S}^s_{-p} & \mathfrak{S}^-_{-p} \end{pmatrix}}_{\mathfrak{S}_p} \cdot \begin{pmatrix} a_+ \\ a_s \\ a_- \end{pmatrix}, \tag{34}$$

where $\mathfrak{S}^s_{-p}$ is zero, as in the fluid no shear stress exists.

The Helmholtz equations eqs (21)–(23) together with the displacement eqs (27)–(30) and stress eqs (31)–(34) components describe the propagation of waves in a cylindrical, poroelastic layer. They are presented in a way that it is possible to formulate an eigenvalue problem which gives for a given frequency ω the axial wavenumber k_z as the eigenvalue. Presented in this form the displacement and stress components eqs (27)–(34) can be utilized to incorporate any boundary and interface conditions for cylindrical poroelastic structures.

2.3 Boundary conditions on poroelastic interfaces

For finite cylindrical structures with arbitrary fluid, solid and poroelastic layers, conditions of continuity across the layer interfaces have to be introduced as well as boundary conditions on the free surface.

For poroelastic interfaces the relevant conditions to be discussed are (Deresiewicz & Skalak 1963; Gurevich & Schoenberg 1999):

(i) poroelastic/poroelastic ($p_1 - p_2$),
(ii) poroelastic/solid ($p - s$),
(iii) poroelastic/fluid ($p - f$).

For case (i) ($p_1 - p_2$) all stress and displacement components, are assumed to be continuous therefore

$$\begin{aligned} & u_r|_{p1} = u_r|_{p1}, \qquad u_z|_{p1} = u_z|_{p2}, \qquad w_r|_{p1} = w_r|_{p2} \\ & \sigma_{rr}|_{p1} = \sigma_{rr}|_{p2}, \qquad \sigma_{rz}|_{p1} = \sigma_{rz}|_{p2}, \qquad p|_{p1} = p|_{p2}. \end{aligned} \tag{35}$$

Case (ii) ($p - s$) is governed by the following conditions:

$$\begin{aligned} & u_r|_p = u_r|_s, \qquad u_z|_p = u_z|_s, \qquad w_r|_p = 0, \\ & \sigma_{rr}|_p = \sigma_{rr}|_s, \qquad \sigma_{rz}|_p = \sigma_{rz}|_s. \end{aligned} \tag{36}$$

All quantities are continuous across the interface except the relative displacement w_r which is zero in the solid.

For case (iii) ($p - f$) two cases have to be considered. Either the pores are open and fluid freely moves across the interface (open pores) or they are closed and no fluid flow can exchange between both layers (closed pores). For both cases the continuity of radial stress and the radial displacement is required as well as the vanishing of the shear stress in the fluid

$$\sigma_{rr}|_p = \sigma_{rr}|_f, \qquad \sigma_{rz}|_p = 0, \qquad u_r|_p - w_r|_p = u|_f. \tag{37}$$

The index f indicates a fluid layer. For the open pores case, the fluid pressure is continuous across the surface

$$p|_p = p|_f, \tag{38}$$

while in the closed pores case the relative displacement is zero in the fluid layer

$$w_r|_p = 0. \tag{39}$$

The conditions of interfaces between solid–solid, solid–fluid and fluid–fluid media are given in Karpfinger *et al.* (2008a).

In addition, surface boundary conditions on the outside layer of the cylindrical structure must be set. Open-pore boundary conditions on the free surface of the cylinder $r = a$ are

$$\sigma_{rr}|_{r=a} = \sigma_{rz}|_{r=a} = -p_f|_{r=a} = 0. \tag{40}$$

In addition to the zero stress, the fluid pressure is zero on the surface and fluid can thus flow across the interface. For a closed surface, the boundary conditions become

$$\sigma_{rr}|_{r=a} = \sigma_{rz}|_{r=a} = 0, \quad w_r|_{r=a} = 0. \tag{41}$$

The pore pressure condition is replaced by the condition that relative motion of fluid with respect to solid is zero on the surface of the cylinder. For a single poroelastic cylinder these boundary conditions are discussed by Berryman (1983) and Karpfinger *et al.* (2008b).

3 SPECTRAL METHOD

The spectral method is an alternative numerical approach to obtain the dispersion and attenuation of modes propagating in cylindrical structures. This method was initially introduced for axisymmetric waves in elastic cylindrical structures by Karpfinger *et al.* (2008a). In this approach, the cylindrical structure is discretized globally using Chebyshev points while differential operators are computed using differentiation matrices (Weideman & Reddy 2000; Adamou & Craster 2004). The eqs (21)–(23) have to be individually discretized for each poroelastic layer using Chebyshev points as well as differentiation matrices. For the case of a free poroelastic cylinder, the dispersion of the axisymmetric modes has been presented by Karpfinger *et al.* (2008b). In this paper we extend this approach for an arbitrary number of fluid, elastic and poroelastic layers. In the following sections it is outlined how the generalized matrix eigenvalue problem is formulated for n-layers. Finally, the computation of the phase velocities and attenuation from the computed eigenvalues is explained.

3.1 Eigenvalue problem for multiple layers

The $\mathfrak{L}_p$-matrix eq. (23) can be combined with the matrix equations of a fluid layer $\mathfrak{L}_f$ or a solid layer $\mathfrak{L}_s$ for any number n of layers in the following form:

$$\underbrace{\begin{pmatrix} \mathfrak{L}_{\xi_1} & 0 & 0 & 0 \\ 0 & \mathfrak{L}_{\xi_2} & 0 & 0 \\ & & \ddots & \\ 0 & 0 & & 0 \\ 0 & 0 & 0 & \mathfrak{L}_{\xi_n} \end{pmatrix}}_{L} \underbrace{\begin{pmatrix} a_{\xi_1} \\ a_{\xi_2} \\ \vdots \\ a_{\xi_n} \end{pmatrix}}_{\boldsymbol{\Theta}} = k_z^2 \begin{pmatrix} a_{\xi_1} \\ a_{\xi_2} \\ \vdots \\ a_{\xi_n} \end{pmatrix}, \tag{42}$$

where $\xi = p, f, s$ stands, respectively, for a poroelastic, fluid or solid layer.

The differential operators $\mathfrak{L}_{\xi_n}$ are discretized for each layer using the $\boldsymbol{r}$ vector as well as the differentiation matrices. The discretization of the differential operators is done the same way as for the elastic case (Karpfinger *et al.* 2008a, sec. III A).

To solve this eigenvalue problem, the interface conditions eqs (25)–(39) for each layer of the system are introduced, as well as open- or closed-pore boundary conditions on the surface of the structure.

3.2 Boundary conditions

The matrix for the stress S and the displacements T for a multilayered system are constructed as presented in eq. (42). The boundary conditions for poroelastic interfaces discussed above are introduced into the eigenvalue problem eq. (42) in a similar manner to how they were introduced for fluid and elastic layers in Karpfinger *et al.* (2008a, sec. IV). In Karpfinger *et al.* (2009), it is illustrated for the case of a fluid-filled borehole surrounded by a poroelastic formation how the interface boundary conditions are set.

Stress and displacement coefficient components corresponding to the boundary conditions are introduced in lines of eq. (42) which correspond to the collocation points of the inner and outer surfaces of each layer. A diagonal matrix Q is constructed where elements corresponding to lines with boundary condition coefficients are set to zero. For more information regarding this construction, the reader can refer to Karpfinger *et al.* (2009) where it is explained in detail how the boundary conditions are set for a fluid-poroelastic interface.

After setting all boundary conditions, the following eigenvalue problem needs to be solved

$$\tilde{L}\boldsymbol{\Theta} = k_z^2 Q \boldsymbol{\Theta}, \tag{43}$$

where $\tilde{L}$ is the L matrix from eq. (42) with coefficients of the boundary conditions introduced in the corresponding lines. Eigenvalues are the squared wavenumbers k_z^2 while phase velocities can be obtained from their real part as

$$v_{ph} = \frac{\omega}{\mathfrak{Re}(k_z)}. \tag{44}$$

The corresponding attenuation Q^{-1} is defined as

$$Q^{-1} = \frac{\mathfrak{Im}(k_z)}{\mathfrak{Re}(k_z)}. \tag{45}$$

Solving this generalized eigenvalue problem (eq. 43) for a range of frequencies allows the computation of the dispersion and attenuation of all modes propagating in the considered structure.

Eigenvectors corresponding to the displacement potentials $\boldsymbol{\Theta}$ can be used to compute the radial distribution of the displacement and stress components. This can be done by multiplying the potential vectors for each mode with the corresponding matrix coefficients of stresses S and displacements T.

4 APPLICATION TO BOREHOLE ACOUSTIC

In borehole acoustics it is of great importance to model dispersion of guided modes such as tube and flexural waves (Schmitt 1988a; Sinha & Asvadurov 2004). In this paper, our focus is on tube waves propagating in a fluid-filled borehole surrounded by a layered poroelastic formation. Tube wave signatures are sensitive to mobility of the surrounding formation e.g. (Chang *et al.* 1988; Liu 1988; Norris 1989; Paillet & Cheng 1991).

In the following section we discuss three well-known examples from borehole acoustics, computed with the spectral method. In all three models we have a layered poroelastic cylinder of radius 2 m, with a fluid-filled borehole in the centre (radius: 0.1 m). Because the radius of the structure is 20 times the radius of the borehole, the tube wave signatures are the same as for infinite formation. The formation, borehole fluid and pore fluid parameters are described in Table 1. Note that the borehole fluid as well as the pore fluid have the same properties.

The first example discussed is a fluid-filled borehole surrounded by a poroelastic formation. This example is widely discussed in literature, for example (Chang *et al.* 1988; Liu 1988; Norris 1989; Paillet & Cheng 1991) and we use the results to benchmark the solution obtained with the spectral method. Dispersion and attenuation for closed- and open-pore boundary conditions are computed and displayed. The second example is a more complex three-layer model with an elastic layer sandwiched between the fluid and the poroelastic formation. In the existing literature only a few models with poroelastic structures existing of more than two layers are discussed (Schmitt 1988b; Liu & Johnson 1997). Using the spectral method, the computation of waves propagating in a three-layer model is straightforward. The third example considers an altered zone around the borehole which has a radius of to 2–3 borehole diameters. This zone will be modelled as layers with reduced permeability. This zone is altered by the drilling process and thus has reduced permeability (Sinha *et al.* 2006). A similar model using a three-layer model (fluid–altered zone–formation) has been already discussed by Schmitt (1988b). Here we consider a radial increase of the permeability by dividing the altered zone in up to eight sublayers. This requires us to obtain the dispersion for a system with up to 10 layers which can be solved using the spectral method in less than 1 min.

4.1 Fluid-filled borehole surrounded by poroelastic formation

First, let us consider the dispersion and attenuation of a tube wave in a borehole surrounded by a poroelastic medium. An analytical low-frequency approximation as well as the exact solution are discussed in Chang *et al.* (1988) and Norris (1989). In Karpfinger *et al.* (2009) the exact solution is computed with the spectral method and is compared to the low-frequency approximation proposed by Chang *et al.* (1988) in the case of open-pore boundary conditions. For the closed-pore boundary conditions case, numerical results were compared to the equivalent Gassmann model obtained with the elastic spectral method (Karpfinger *et al.* 2008a). Here the influence of the formation mobility on the dispersion curve is illustrated. Fig. 2 presents dispersion curves computed for a range of permeabilities from 1 mD to 1000 mD and a frequency range from 1 Hz to 5000 Hz. When the permeability is decreasing, the low frequencies part of the dispersion curve decreases and is, at 1 mD, almost indistinguishable from the closed boundary condition case.

Table 1. Material parameters of the formation used for all discussed examples.

Grain density	$\rho_{\text{grain}} = 2875\,\text{kg m}^{-3}$
Shear modulus	$G = 8.85$ GPa
Drained bulk modulus	$K = 10.8$ GPa
Grain modulus	$K_g = 48$ GPa
Viscosity	$\eta = 10^{-3}$ Pa s
Tortuosity	$a_\infty = 1.91$
Fluid density	$\rho_f = 1000\,\text{kg m}^{-3}$
Porosity	$\phi = 0.2$
Fluid bulk modulus	$K_f = 2.3$ GPa
Permeability	$\kappa = 1\text{D}$

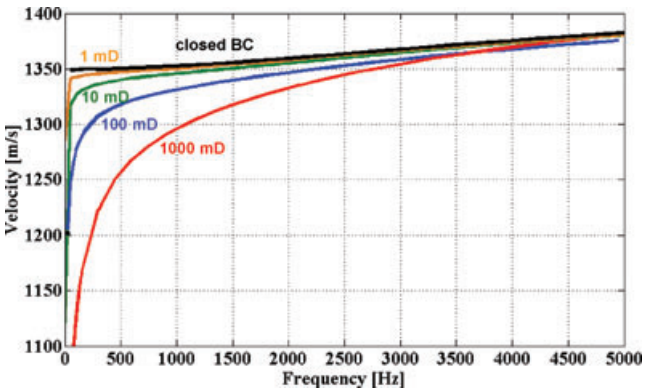

Figure 2. Tube wave dispersion in a fluid-filled borehole surrounded by a poroelastic formation; top curve shows poroelastic formation with closed boundary conditions; other curves correspond to open boundary conditions with varying permeabilities.

For high frequencies, the dispersion curve for 1000 mD has higher velocities compared to the one computed for lower permeabilities. For high enough frequencies tube wave for open-pore boundary condition travels faster than the tube wave for the equivalent elastic medium (closed BC). Qualitatively it is observed that for increasing permeability the frequency where the elastic dispersion equals the poroelastic dispersion shifts towards lower frequencies. This result can be understood because the high-frequency limit of the tube wave in a poroelastic formation tends towards the Scholte velocity of a fluid-poroelastic interface which is faster than its elastic equivalent (Feng & Johnson 1983). In Fig. 3 the attenuation Q^{-1} as a function of frequency is plotted for the same model. Here it can be observed

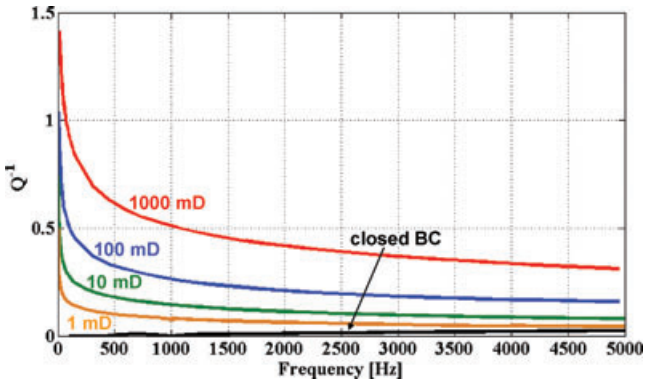

Figure 3. Tube wave attenuation in a fluid-filled borehole surrounded by a poroelastic formation; bottom curve shows poroelastic formation with closed boundary conditions; other curves correspond to open boundary conditions with varying permeabilities.

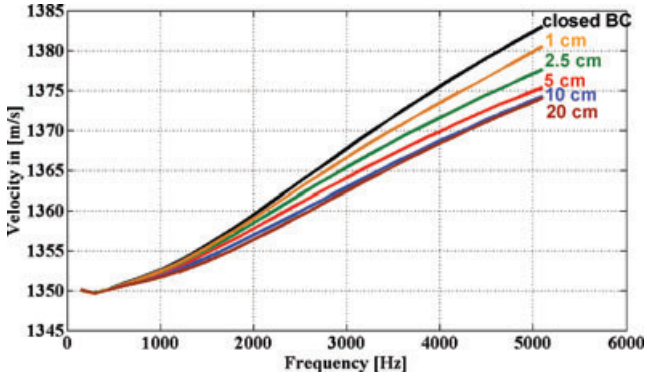

Figure 4. Tube-wave dispersion for an elastic layer with varying thickness sandwiched between the fluid and the poroelastic layer; top curve: two layer case fluid-poroelastic with close-pore boundary conditions on the interface; increasing thickness of sandwiched elastic layer show decrease of tube wave velocity; for thicknesses bigger than 20 cm the dispersion is only guided by the properties of the elastic layer.

that for decreasing permeability the attenuation gets smaller. For closed boundary conditions the attenuation is zero.

4.2 Effect of an elastic layer between fluid and poroelastic formation

The second example investigates the effect of the thickness of an elastic layer sandwiched between the fluid-filled borehole and the poroelastic formation. For the elastic layer we have used the Gassmann velocities of the poroelastic formation. For a very thin elastic layer the dispersion is equivalent to the case of closed-pore boundary conditions. The pores on the borehole wall are effectively closed and no fluid flow can occur, therefore the dispersion is the same as for an equivalent elastic model. The dispersion due to closed boundary conditions is compared to the dispersion with an elastic layer. The effect of the thickness of the elastic layer is considered especially.

In Fig. 4 the dispersion of a tube wave propagating for such a model is illustrated.

The thickness of the elastic layer ranges from 0 cm (closed BCs) to 20 cm. At low frequencies all dispersion curves tend towards the same limit, that is, the low-frequency limit of tube waves propagating in a borehole surrounded by an elastic formation. One drawback of the spectral method becomes visible here; the results for low frequencies become numerically unstable and the dispersion curves are not perfectly smooth. Nevertheless the low-frequency limit can still be estimated reasonably well. At high frequencies the thickness of the elastic layer causes a difference in the observed dispersion. For layer thicknesses of 5 cm the difference with the closed boundary conditions case is approximately 8 $\mathrm{m\,s^{-1}}$. As the thickness of the elastic layer becomes bigger than 5 cm the tube wave signatures do not significantly change anymore and are therefore not influenced by the surrounding poroelastic formation.

4.3 Effect of an altered zone between fluid and poroelastic formation

Reservoir engineers know well that altered zone around boreholes often experiences 'formation damage' (i.e. permeability reduction). In some cases an altered zone can have distinct mechanical properties, but almost always it suffers from a permeability reduction

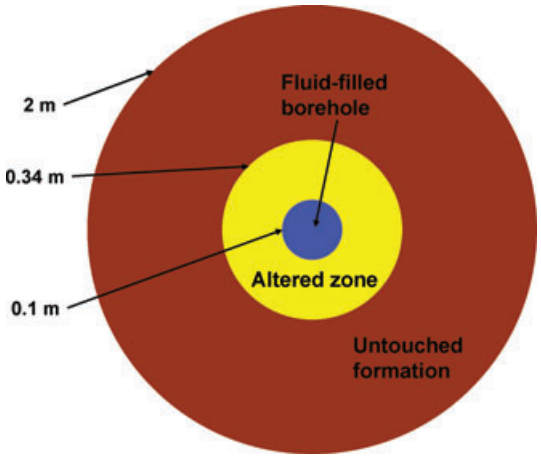

Figure 5. Geometry of the model of a borehole surrounded by a invaded zone of reduced permeability and an untouched formation.

due to mechanical and chemical factors caused by well drilling and completion processes. Permeability reduction causes problems when extracting oil and gas from hydrocarbon reservoirs. The problem of an altered zone with reduced permeability has been discussed by various authors (Schmitt 1988b; Sinha *et al.* 2006).

The last example considers a borehole surrounded by such an altered zone. The geometry is illustrated in Fig. 5, where the altered zone has a thickness of 0.24 m. To consider the effect of the reduced permeability on the tube wave signatures, a radial change in permeability is included. In Fig. 6 the black curve represents the dispersion of a tube wave in a borehole surrounded by an unaltered formation with a permeability of 1000 mD. The curves in magenta, green and red take the effect of the altered zone into account with different radial permeability profiles. The magenta curve is the dispersion considering an altered zone as a single layer with a permeability of 200 mD. The green dispersion curve was computed for an invaded zone composed of four layers of 6 cm thickness with a permeability increasing stepwise (200 mD, 400 mD, 600 mD and 800 mD). The red line separates the invaded zone into eight layers of 3 cm thickness where the radial change in permeability is (200 mD, 300 mD, 400 mD, 500 mD, 600 mD, 800 mD and 900 mD).

As one can see, there is a significant change in dispersion from no invaded to an invaded zone with one layer and a permeability

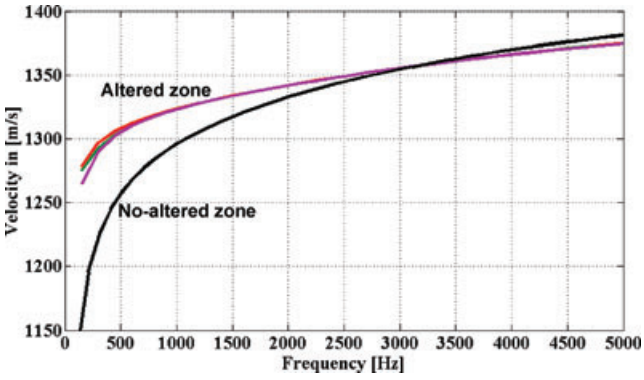

Figure 6. Tube wave dispersion of a borehole surrounded by an invaded zone of reduced permeability and an untouched formation; altered zone has a thickness of 24 cm; we consider several models which consist of no (black), single (violet), four (green) and eight (red) sublayers of equal thickness; in all cases the permeability of the inner layer is 200 mD.

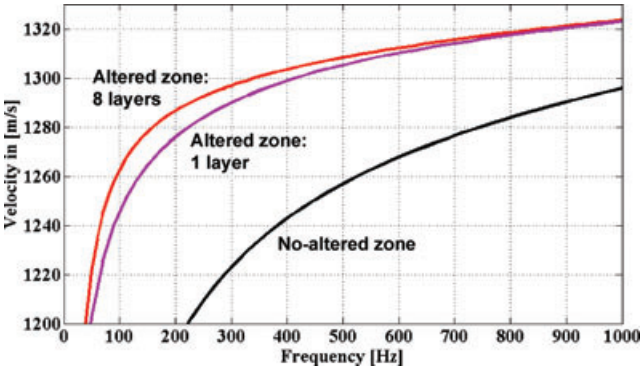

Figure 7. Same as Fig. 6 but zoomed in for low frequencies; displayed here is an invaded zone with a single sublayer (violet) and eight (red) sublayers; the effect of the sublayers is most significant for frequencies between 100 Hz and 400 Hz; in all cases the permeability of the inner layer is 200 mD.

reduced to 200 mD. However, for a radial permeability change within the invaded zone the difference between one and eight layers is not significant. The fluid flow causing the tube wave dispersion mostly depends on the permeability of the layer adjacent to the borehole, therefore the flow between the different poroelastic layers does not significantly influence the tube wave dispersion.

In Fig. 7 the dispersion curve for an altered zone with one internal layer is compared to the eight-layer case. On a smaller scale it becomes obvious that for a frequency range from 100 Hz to 400 Hz the difference is up to 10 m s^{-1}. It might be possible to use this low-frequency range to invert for the radial distribution of the permeability.

5 CONCLUSIONS

In this study we have introduced a new numerical approach called the spectral method which allows the computation of mode signatures propagating in a fluid-filled borehole surrounded by a cylindrically layered poroelastic formation. The fundamental equations for cylindrical poroelastic structures are derived on the basis of Biot's theory and presented in the context of the spectral method. It is outlined how these equations are used to construct a generalized matrix eigenvalue problem for an arbitrary number of fluid, elastic and poroelastic layers. To illustrate the numerical scheme, we discussed three examples from borehole acoustics. First we validated the spectral method on a well-known example of fluid-filled borehole surrounded by a poroelastic medium. Two remaining examples illustrated cases with additional cylindrical layering of up to 10 layers. The number of layers was no limitation for the spectral method and could still be computed very time efficiently (in less than 1 min).

The spectral method successfully allows obtaining the dispersion for all examples easily and time efficiently. It has been shown that the spectral method is a very powerful alternative method for the computation of wave propagation in complicated poroelastic structures. This provides the opportunity to obtain more accurate descriptions of realistic borehole conditions and thus achieve a better characterization of petrophysical properties of subsurface formations.

Future work can be focused on the implementation of absorbing boundary conditions to model a real infinite medium. This will also allow obtain the dispersion of leaky modes and eliminates higher order modes that only propagate in finite structures. Absorbing boundary conditions will also help to reduce the number of collocation points. In the example with the altered zone only one parameter, the permeability, was changed. It would be of interest to see how the dispersion would be influenced if various parameters were changed such as, for example, the shear modulus. This, as well as, for example, the effect of anisotropic media can also be considered in the future.

ACKNOWLEDGMENTS

We are grateful to Boris Kashtan (St. Petersburg State University, Russia) who suggested the idea of applying the spectral method to the problem at hand and Richard Craster (Imperial College, London) for helpful advice. We greatly appreciate discussion with David L. Johnson (Schlumberger-Doll Research). Florian Karpfinger thanks Shell International Exploration and Production Inc. for support of his Ph.D. project.

REFERENCES

Adamou, A.T.I. & Craster, R.V., 2004. Spectral methods for modelling guided waves in elastic media, *J. acoust. Soc. Am.,* **116**(3), 1524–1535.

Berryman, J.G., 1983. Dispersion of extensional waves in fluid-saturated porous cylinders at ultrasonic frequencies, *J. acoust. Soc. Am.,* **74**(6), 1805–1812.

Berryman, J.G. & Pride, S.R., 2005. Dispersion of waves in porous cylinders with patchy saturation: formulation and torsional waves, *J. acoust. Soc. Am.,* **117**(4), 1785–1795.

Biot, M.A., 1956a. Theory of propagation of elastic waves in a fluid-saturated porous solid. I. Low-frequency range, *J. acoust. Soc. Am.,* **28,** 168–178.

Biot, M.A., 1956b. Theory of propagation of elastic waves in a fluid-saturated porous solid. II. Higher frequency range, *J. acoust. Soc. Am.,* **28,** 179–191.

Biot, M.A., 1962. Generalized theory of acoustic propagation in porous dissipative media, *J. acoust. Soc. Am.,* **34**(5), 1254–1264.

Biot, M.A. & Willis, D.G., 1957. The elastic co-efficients of the theory of consolidation, *J. appl. Mech.,* **24,** 594–601.

Chang, S.K., Liu, H.L. & Johnson, D.L., 1988. Low-frequency tube waves in permeable rocks, *Geophysics,* **53**(4), 519–527.

Deresiewicz, H. & Skalak, R., 1963. On uniqueness in dynamic poroelasicity, *Bull. seism. Soc. Am.,* **53,** 783–788.

Dunn, K.-J., 1986. Acoustic attenuation in fluid-saturated porous cylinders at low frequencies, *J. acoust. Soc. Am.,* **79**(6), 1709–1721.

Feng, S. & Johnson, D.L., 1983. High-frequency acoustic properties of a fluid/porous solid interface. I. New surface mode, *J. acoust. Soc. Am.,* **74**(3), 906–914.

Gardner, G.H.F., 1962. Extensional waves in fluid-saturated porous cylinders, *J. acoust. Soc. Am.,* **34**(1), 36–39.

Gassmann, F., 1951. Über die elastizität poröser medien, *Viertel. Naturforsch. Ges. Zürich,* **96,** 1–23.

Gurevich, B. & Schoenberg, M., 1999. Interface conditions for biot's equations of poroelasticity, *J. acoust. Soc. Am.,* **105,** 2585–2589.

Johnson, D.L., Koplik, J. & Dashen, R., 1987. Theory of dynamic permeability and tortuosity in fluid-saturated porous media, *J. Fluid Mech.,* **176,** 379–402.

Karpfinger, F., Gurevich, B. & Bakulin, A., 2008a. Computation of wave propagation along cylindrical structures using the spectral method, *J. acoust. Soc. Am.,* **124**(2), 859–865.

Karpfinger, F., Gurevich, B. & Bakulin, A., 2008b. Modeling of axisymmetric wave modes in a poroelastic cylinder using spectral method, *J. acoust. Soc. Am.,* **124**(4), EL230–EL235.

Karpfinger, F., Gurevich, B. & Bakulin, A., 2009. Axisymetric waves in fluid saturated porous structures, in *Poromechanics IV, Proceedings of the 4th Biot Conference on Poromechanics,* pp. 625–630, Lancaster, PA, DEStech Publications.

Karpfinger, F., Valero, H.-P., Gurevich, B., Bakulin, A. & Sinha, B., 2010. Spectral method algorithm for modeling dispersion of acoustic modes in elastic cylindrical structures, *Geophysics,* **75**(3), H19–H27.

Liu, H.-L., 1988. Borehole modes in a cylindrical fluid-saturated permeable medium, *J. acoust. Soc. Am.,* **84**(1), 424–431.

Liu, H.-L. & Johnson, D.L., 1997. Effects of an elastic membrane on tube waves in permeable formations, *J. acoust. Soc. Am.,* **101**(6), 3322–3329.

Mörig, R. & Burkhardt, H., 1989. Experimental evidence for the Biot-Gardner theory, *Geophysics,* **54**(4), 524–527.

Norris, A.N., 1989. Stoneley-wave attenuation and dispersion in permeable formations, *Geophysics,* **54**(3), 330–341.

Paillet, F.L. & Cheng, C.H., 1991. *Acoustic Waves in Boreholes,* Boca Raton, CRC Press.

Pride, S.R. & Haartsen, M.W., 1996. Electroseismic wave properties, *J. acoust. Soc. Am.,* **100**(3), 1301–1315.

Rosenbaum, J.H., 1974. Synthetic microseismograms: logging in porous formations, *Geophysics,* **39,** 14–32.

Schmitt, D.P., 1988a. Shear wave logging in elastic formations, *J. acoust. Soc. Am.,* **84**(6), 2215–2229.

Schmitt, D.P., 1988b. Effects of radial layering when logging in saturated porous formations, *J. acoust. Soc. Am.,* **84**(6), 2200–2214.

Schmitt, D.P., Zhu, Y. & Cheng, C.H., 1988. Shear wave logging in semi-infinite saturated porous formations, *J. acoust. Soc. Am.,* **84**(6), 2230–2244.

Sinha, B. & Zeroug, S., 1997. Geophysical prospecting using sonics and ultrasonics, in *Wiley Encyclopedia of Electrical and Electronic Engineers,* Wiley, New York.

Sinha, B.K. & Asvadurov, S., 2004. Dispersion and radial depth of investigation of borehole modes, *Geophys. Prospect.,* **52**(4), 271–286.

Sinha, B.K., Vissapragada, B., Renlie, L. & Tysse, S., 2006. Radial profiling of the three formation shear moduli and its application to well completions, *Geophysics,* **71**(6), E65–E77.

Weideman, J.A.C. & Reddy, S.C., 2000. A MATLAB differentiation matrix suite, *ACM Trans. Math. Softw.,* **26,** 465–519.

White, J.E., 1983. *Underground Sound: Application of Seismic Waves,* New York, Elsevier.

White, J.E., 1986. Biot-Gardner theory of extensional waves in porous rods, *Geophysics,* **51**(3), 742–745.